

Title	Interdigitating organic bilayers direct the short interlayer spacing in hybrid organic–inorganic layered vanadium oxide nanostructures
Authors	Gannon, G.; O'Dwyer, Colm; Larsson, J. Andreas; Thompson, Damien
Publication date	2011-10-31
Original Citation	Gannon, G., O'Dwyer, C., Larsson, J. A. and Thompson, D. (2011) 'Interdigitating organic bilayers direct the short inter layer spacing in hybrid organic-inorganic layered vanadium oxide nanostructures'. Journal of Physical Chemistry B, 115(49), pp. 14518–14525. http://dx.doi.org/10.1021/jp207709c
Type of publication	Article (peer-reviewed)
Link to publisher's version	10.1021/jp207709c
Rights	© 2011 American Chemical Society. This document is the Accepted Manuscript version of a Published Work that appeared in final form in The Journal of Physical Chemistry B, copyright © American Chemical Society after peer review and technical editing by the publisher. To access the final edited and published work see http://pubs.acs.org/doi/abs/10.1021/jp207709c
Download date	2024-04-26 05:22:54
Item downloaded from	https://hdl.handle.net/10468/2812



UCC

University College Cork, Ireland
Coláiste na hOllscoile Corcaigh

Interdigitating Organic Bilayers Direct the Short Interlayer Spacing in Hybrid Organic-Inorganic Layered Vanadium Oxide Nanostructures

Journal:	<i>The Journal of Physical Chemistry</i>
Manuscript ID:	jp-2011-07709c.R1
Manuscript Type:	Article
Date Submitted by the Author:	25-Oct-2011
Complete List of Authors:	Gannon, Greg; Universität Bern, Laboratory of Computational Chemistry and Biochemistry O'Dwyer, Colm; Materials and Surface Science Institute, Department of Physics Larsson, J.; University College Cork, National Microelectronics Research Centre Thompson, Damien; Tyndall National Institute, Computational Modelling Group

SCHOLARONE™
Manuscripts

1
2 **Interdigitating Organic Bilayers Direct the Short Interlayer Spacing in Hybrid Organic-Inorganic**
3
4 **Layered Vanadium Oxide Nanostructures**
5

6
7 *G. Gannon^{1,2}, C. O'Dwyer^{3*}, J. A. Larsson¹ and D. Thompson^{1*}.*
8

9 ¹Theory Modelling and Design Centre, Tyndall National Institute, University College Cork, Cork,
10 Ireland. ²Current address: Laboratory of Computational Chemistry and Biochemistry, Departement für
11 Chemie und Biochemie, Universität Bern, Freiestrasse 3, CH-3012 Bern, Switzerland. ³Department of
12 Physics and Energy, and Materials and Surface Science Institute, University of Limerick, Limerick,
13
14
15
16
17
18
19 Ireland.

20
21 *Corresponding authors: damien.thompson@tyndall.ie; colm.odwyer@ul.ie.
22
23
24
25
26
27
28
29
30
31
32
33
34
35
36
37
38
39
40
41
42
43
44
45
46
47
48
49
50
51
52
53
54
55
56
57
58
59
60

1
2 **Abstract:** Layered metal oxides provide a single-step route to sheathed superlattices of atomic
3
4 layers of a variety of inorganic materials, where the interlayer spacing and overall layered structure
5
6 forms the most critical feature in the nanomaterials' growth and application in electronics, health
7
8 and energy storage. We use a combination of computer simulations and experiments to describe the
9
10 atomic-scale structure, dynamics and energetics of alkanethiol-intercalated layered vanadium oxide-
11
12 based nanostructures. Molecular dynamics (MD) simulations identify the unusual substrate-
13
14 constrained packing of the alkanethiol surfactant chains along each V_2O_5 (010) face that combines
15
16 with extensive interdigitation between chains on opposing faces to maximise three-dimensional
17
18 packing in the interlayer regions. The findings are supported by high resolution electron microscopy
19
20 analyses of synthesized alkanethiol-intercalated vanadium oxide nanostructures and the preference
21
22 for this new interdigitated model is clarified using a large set of MD simulations. This dependency
23
24 stresses the importance of organic-inorganic interactions in layered material systems, the control of
25
26 which is central to technological applications of flexible hybrid nanomaterials.
27
28
29
30
31

32
33 **Keywords:** hybrid hard-soft materials; organic-inorganic interfaces; metal oxide; alkanethiol self-
34
35 assembly; electron microscopy; molecular dynamics.
36
37
38
39
40
41
42
43
44
45
46
47
48
49
50
51
52
53
54
55
56
57
58
59
60

Introduction

Many emerging applications of nanostructures involve organic molecules adsorbed on inorganic substrates¹. Organic functionalization, monolayer formation and docking onto inorganic substrates has been a key building block interaction that has allowed control over size, shape, physico-chemical properties and assembly. As an important subset to the rational design of many nanostructures through organic-inorganic interactions and assemblies, the role of the surfactant packing and adsorption onto the inorganic phase is crucial in order to influence crystal growth and assembly²⁻³. The vast majority of such interactions concern synthetic control of nanocrystals and nanowires, but incorporation of these structure-influencing organic layers *into* the crystals such as layered double hydroxides⁴ and layered metal oxide materials is mostly limited to variations in the type of organic intercalant, and much less is known about the influence of this phase and its interaction on the overall layered material. The advantage of template-based growth methods is the ability of fabricating unidirectionally aligned and uniformly sized nanostructured arrays. To this end, the direct engineering of complex nanostructures is highly desirable, but controlled hierarchical structuring of choice materials remains challenging⁵⁻⁶.

Layered metal oxides with characteristic morphologies similar to single crystal nanostructures, such as nanofibers, provide a single-step route to sheathed superlattices of atomic layers of inorganic material⁷ and have applications ranging from energy-storage, display devices, (photo)electrochromic devices, electrocatalysis and photovoltaics, to novel energy-conversion systems, proton-pump electrodes and sensors, for example chemiresistive “artificial nose” detectors⁸⁻¹³. The motivation for the present study stems from the considerable attention that these layered nanostructures are currently receiving¹⁴ coupled to the limited knowledge on the true effect of intercalated organic monolayers on structure and physicochemical properties¹⁵⁻¹⁷. Vanadium oxide is re-emerging with renewed interest, based on its layered architecture and the possibility of its application to energy storage and conversion¹⁸ among many other beneficial properties¹⁹. For example, the influence of the ‘soft’ organic phase was shown to influence specific charge capacity and cycle life in vanadate-based lithium-ion battery materials¹³. As a

1
2 layered transition metal oxide, it also serves as a model material for hybrid organic-inorganic
3
4 nanomaterial investigations.
5

6
7 In the present work, we resolve the structure of alkanethiol-vanadium oxide hybrid materials,
8
9 both experimentally and theoretically. We use a combination of electron microscopy imaging and
10
11 atomic-resolution molecular dynamics simulations to clarify the role of surfactant molecules in the
12
13 assembly of layered metal oxide nanostructures, which go beyond known experimental and
14
15 computational tandem approaches that primarily focused on phase changes in the ‘harder’ inorganic
16
17 phase²⁰. We show that alkanethiol molecules self-assemble preferentially in a vertically-interdigitated,
18
19 bilayered arrangement between the layers comprising the vanadium oxide-based nanostructures.²¹ The
20
21 findings demonstrate that a controlled interlayer spacing in a layered material can be obtained by the
22
23 incorporation of the organic bilayer. The interlayer spacing is dependent not only on the length of the
24
25 alkyl chain and how they interact, but on the density of organic molecules on the surface of the inorganic
26
27 phase and how the overall packing density maintains interlayer spacing throughout the layer, even when
28
29 grown as a superlattice of many organic-inorganic bilayers stacked periodically back-to-back.
30
31
32
33
34
35
36

37 **Methods**

38 Characterization of vanadium oxide-alkanethiol nanofibers

39
40
41
42 Details on the synthesis of the vanadium oxide-thiol nanofibers are outlined in detail elsewhere²¹⁻²². X-
43
44 ray powder diffraction characterization was performed using a SIEMENS D5000 diffractometer (Cu K α
45
46 = 0.15418 nm, operation voltage 40 kV, current 30 mA). Transmission electron microscopy (TEM) was
47
48 conducted using a JEOL 2100F FEGTEM operating at 200 kV. X-ray photoelectron spectroscopy was
49
50 performed using a Kratos Axis 165 equipped with a monochromatic Al source (K α 1486.58 eV) with a
51
52 spot size of 1 mm. The source power was 150 W, the take-off angle was set normal to the sample
53
54 surface, the construction and peak fitting in the narrow region spectra was performed using a Shirley
55
56
57
58
59
60

1
2 type background, and the synthetic peaks were of a mixed Gaussian Lorentzian type. Adventitious
3
4 carbon was used for charge reference, and the C 1s line of adventitious hydrocarbon was assumed to
5
6 have a binding energy of 284.8 eV. After synthesis, dried xerogel samples comprising nanofibers were
7
8 stored under 1 atm with a relative humidity of 40%. No humidity control was used during analytical
9
10 (diffraction/microscopic) measurements due to vacuum requirements.
11
12

13 14 15 16 Choice of thiol-substrate binding sites

17
18 Three alternative grafting arrangements were considered in the molecular models (Figure 1), differing in
19
20 the (experimentally unknown) local distribution of thiol attachment sites. The molecule-surface
21
22 attachment sites on the V_2O_5 substrate in the model involve the thiol headgroups binding via the
23
24 negatively-charged S atom to the vanadium Lewis acid sites at the V_2O_5 (010) surface²³ and so we
25
26 bound alkanethiols to sterically-accessible vanadium sites, those without a doubly-bound oxygen sitting
27
28 on top. There are many other possibilities, involving alternative surface binding sites as a consequence
29
30 of, for example, thiol molecules adsorbing via -SH instead of -S headgroups to doubly-bonded vanadyl
31
32 oxygens and/or surface in-plane nucleophilic oxygens²⁴, oxygen vacancies, surface V^{5+}/V^{4+} ratios and
33
34 new surface states formed following, for example, condensation reactions²⁵.
35
36
37
38
39

40 The representative model we chose may also serve as a first approximation to the alternative
41
42 *alkylamine*- V_2O_5 lamellar structure²¹, the doubly-bonded vanadyl oxygens serving as likely candidates
43
44 for NH_3^+ binding sites. In Supporting Information Figure S1 we show a HRTEM image of the layered
45
46 walls of a dodecylamine-templated V_2O_5 nanotube^{13,26} which routinely show an interlayer spacing of
47
48 2.65-2.7 nm. The increase in interlamellar separation from 2.5 (thiol templated) to ~2.7 nm (amine
49
50 templated) corresponds to an increase of 1-2 V=O bond lengths. Hence a similar film horizontal "lattice
51
52 constant" may be expected for alkyl amines as for alkanethiols. Note however the further discussion of
53
54 the lamellar structural features associated with more mobile ionic, *e.g.*, NH_3^+ , anchor groups in reference
55
56
57
58
59 ²⁷. In common with alkanethiol adsorption described above, alternative film-substrate binding sites are
60

possible also for alkylamines, in particular due to competition^{24,28} between surface Bronsted base V=O and in-plane Lewis base V-O-V oxygens for the amino headgroups.

An important additional model feature is that we restricted ourselves in this study to structures with all alkanethiols chemically bound to the substrate, given the strong energetic benefit of thiol:substrate chemisorption of at least 20 kcal/mol²⁹ which is generally much larger than the magnitude of the film packing effects calculated in this study (Table 1 below). An alternative arrangement could feature bound chains with additional alkanethiols interspersed but not chemically bonded to the V₂O₅ substrate, which could potentially provide a means of attaining the density of the bulk system while adapting to the limitations of the surface, albeit with a significant loss in thiol-surface binding energy. Note finally that we arbitrarily use a single-layer model for the V₂O₅ (010) substrate. Irrespective of the number of layers, which is typically two in synthesized gels²¹, the same two (010) faces will be exposed for chain attachment.

Choice of film density in the molecular models

We use a doubled V₂O₅ unit cell³⁰ (Figure 1a(i)) as the substrate repeat unit in our models, with an area of 2 x 1.148 nm x 0.355 nm = 0.82 nm². Onto this we graft 5 alkanethiols (Figure 1a(ii)), 2 on one face and 3 on the other (Configurations **A** and **B**) or 4 on one face and 1 on the other (Configuration **C**). For an interlamellar spacing of approximately 2.0 nm, giving extreme interdigitation, (Figure 1b), the densities sum to give 5 chains per 0.82 nm² or 6.1 chains/nm².

Figure 1c plots the maximum density available to the surfactant chains in both two- and three-dimensional space. The plot shows that, for interlamellar space > 2.25 nm, each face has a grafting density lower than the 5.5 chains/nm² of a reference water-solvated dodecanethiol bilayer. Details of the water-solvated bilayer model will be presented elsewhere. In the dodecanethiol-V₂O₅ structures, only where the chains from the two layers overlap can one speak of an equivalent of 5 chains per layer (6.1 chains/nm²). In this overlap region the dodecanethiol concentration is higher than elsewhere – this point

1
2 on film inhomogeneity is developed further in Supporting Information section S2. The decrease in
3
4 density towards that of the water-solvated bilayer then directs widening of the interlamellar space; the
5
6 6.1 chain/nm² system at 2.0 nm (Figure 1b) corresponds to an overpacked system as reflected in the film
7
8 energies in Table 1 below. As shown in Figure 1c, the reduced chain densities obtained in expanded
9
10 interlamellar spaces directs the system towards a moderate spacing of 2.26 nm, in reasonable agreement
11
12 with the microscopy image estimates of 2.40-2.55 nm from Figure 2 below. Switching to densities
13
14 expressed in units of g/cm³ to compare with the known density of dodecanethiol bulk liquids, 0.85 g/cm³
15
16 at room temperature from^{31,32}, Figure 1c shows that the three-dimensional chain density at a separation
17
18 of 2.5 nm is 0.82 g/cm³, in very good agreement with the bulk liquid.
19
20
21
22

23 Layering stabilizes the system by increasing the density and maximizing packing. The narrow
24
25 2.0 nm interlamellar spacing gives a three-dimensional density that is approximately the sum of the
26
27 individual densities of the three and two chains on alternating layers giving a total of five chains in the
28
29 interlamellar space. This narrow 2 nm spacing results in overly-cramped intercalated films. At 2.5 nm
30
31 separation the density at either face is lower than the bilayer system while at the interface, or vertical
32
33 center of the bilayer, the density is above the bilayer density. Together these horizontal and vertical
34
35 packing effects combine to provide an overall density that approximates the density of the bulk
36
37 dodecanethiol liquid. The surfactant concentration used in the molecular dynamics models then
38
39 corresponds, at the observed 2.5 nm interlamellar space, to a chain density similar to that of the
40
41 reference systems. That is, it approximates the optimised two- and three-dimensional packing
42
43 arrangements of the water-solvated bilayer and bulk liquid.
44
45
46
47
48
49
50

51 Molecular dynamics protocol

52 Each model was relaxed using 2000 steps of steepest descent minimization with respect to the
53
54 CHARMM force field³³ and then brought to room temperature by gradually raising the temperature from
55
56 0 to 295 K over 2 nanoseconds of dynamics while simultaneously loosening positional constraints on the
57
58
59
60

1
2 alkanethiol chains. Substrate atoms were fixed to their crystallographic positions³⁰ throughout the
3
4 simulations. The crystal structure of V_2O_5 in the $V_2O_5 \cdot nH_2O$ xerogel is very similar³⁴ to the bulk V_2O_5
5
6 structure and it is assumed that atomic positions are also similar. Vanadium and oxygen atoms were
7
8 assigned van der Waals's radii from the V_2O_5 crystal contacts³⁰ with well depths corresponding to
9
10 typical metal and oxygen parameters³⁵. Each of the eleven models listed in main text Table 1 was then
11
12 subjected to five nanosecond (5 ns) dynamics runs to allow formation of well-equilibrated film
13
14 structures. This corresponds to 77 ns of dynamics, composed of 22 ns for equilibration plus 55 ns of
15
16 equilibrated dynamics.
17
18
19

20
21 The NAMD program³⁶ was used to calculate Langevin dynamics with a constant volume-
22
23 temperature ensemble. Periodic boundary conditions were applied with Ewald summation used to
24
25 calculate the electrostatic interactions and a 2 fs timestep used for dynamics by constraining covalent
26
27 bonds to hydrogen via the ShakeH algorithm³⁷. We recently used a similar simulation protocol^{35,38-39} to
28
29 describe alkanethiol self-assembled monolayers on gold⁴⁰. Image generation and Tcl script-based
30
31 trajectory analysis was performed using the VMD program⁴¹. The NAMD³⁶ scripts used for the
32
33 simulations, together with the computed structures, are available on request from the corresponding
34
35 author.
36
37
38
39

40
41 Next-generation models would benefit from (a) a combined quantum/classical approach that
42
43 could simultaneously treat the substrate electronic structure and binding/unbinding of alkanethiols and
44
45 solvent molecules, *while* (b) allowing for dynamic redistribution of alkanethiols between those that are
46
47 chemically-bound, those physisorbed to substrate, and those in bulk-like states outside the fiber, within a
48
49 constant pressure-temperature ensemble. Such complex, large and long simulations are becoming more
50
51 feasible with advances in high-performance computing.
52
53
54

56 Results and Discussion

57 Alkanethiol- V_2O_5 nanofiber characterisation

1
2 Figure 2a shows the as-synthesized V_2O_5 nanofibers. The dried layered fibers were synthesized as
3
4 described above. After mild sonication to debundle the V_2O_5 -thiol nanofibers, plan view transmission
5
6 electron microscopy (TEM) images show the layered nature of these 2-dimensional crystals. Nanofibers
7
8 are found to grow along the [100] direction (Figure 2a,b) and are single crystal in nature, as shown in the
9
10 HRTEM image in Figure 2b, with lattice spacings corresponding to orthorhombic V_2O_5 . Cross-sectional
11
12 analysis of a single nanofiber by HRTEM (Figure 2c), summarized schematically in Figure 2e, clearly
13
14 identifies the ordered layered structure, with well-defined interlayer spacings from this image in the
15
16 range 2.40-2.55 nm. Low angle XRD measurements in Figure 2d confirm this. The diffraction pattern is
17
18 consistent with the intercalation of the alkanethiol surfactant template into the layered matrix to form an
19
20 effective double bilayer sandwich, and shows that the inorganic layered structure of the host xerogel is
21
22 maintained consistent with a topotactic reaction. The (001) reflection for the V_2O_5 -alkanethiol
23
24 compound corresponds to a layer distance of ~ 2.5 nm, with the corresponding (001) reflection for the
25
26 preliminary $V_2O_5 \cdot nH_2O$ xerogel giving a much shorter interlayer spacing of ~ 1.5 nm (due to intercalated
27
28 water). The highly layered nature of the hybrid V_2O_5 -alkanethiol superlattice is observable from Figure
29
30 2d, where superlattice reflections $SL(-1)$ and $SL(+1)$ around a zeroth order $SL(0)$, are found and are
31
32 related to the intercalated bilayered alkanethiols sandwiched periodically between layers of V_2O_5 (010)
33
34 faces⁴². X-ray photoelectron analysis of bulk nanofiber regions where the majority of deposited fibers
35
36 were found to be parallel to the substrate, indicate that they contain $<10\%$ V^{4+} (Supporting Information
37
38 Figure S3), and concentrations of V^{4+} up to 20% within the vanadium oxide layers will not alter the
39
40 crystal structure of the material¹⁹. This suggests effective functionalization of the opposing interlayer
41
42 faces throughout the layer fibers. Finally, HRTEM analysis of fiber surfaces and cross-sections
43
44 (Supporting Information Figure S4) shows a thin 2-5 nm thiol layer at the edges of the nanofibers,
45
46 consistent with non-V-S binding energies in V 2p core level photoelectron spectra, indicating a small
47
48 degree of physisorbed thiols on the outside of the fiber which could stem from mild post-synthetic
49
50 cleaning procedures. Finally, HRTEM analysis of fiber surfaces and cross-sections
51
52 (Supporting Information Figure S4) shows a thin 2-5 nm thiol layer at the edges of the nanofibers,
53
54 consistent with non-V-S binding energies in V 2p core level photoelectron spectra, indicating a small
55
56 degree of physisorbed thiols on the outside of the fiber which could stem from mild post-synthetic
57
58 cleaning procedures.
59
60

Computed structure, dynamics and energetics of the nanofiber

To quantify the effects of interlayer film spacing on the stability of the intercalated film using molecular dynamics simulations, eleven dodecanethiol- V_2O_5 models were used. The models were built with dodecanethiol chains grafted onto the (010) faces of the V_2O_5 crystal unit cell³⁰, in three alternative binding configurations **A** (five models), **B** (four models) and **C** (two models), for a film density of 6.1 chains/nm² (Figure 1). Since the inorganic layers of the vanadium oxide are in fact molecular bilayers themselves⁴², the organic docking surface remains identical with both faces juxtaposed in each interlayer gallery spacing. The 6.1 chains/nm² film density reflects the crystallography of V_2O_5 (010) as described above in Methods. Note that similarly high densities in the range 5.9-6.2 chains/nm² have been observed in alkanethiol assembly experiments on silver and gold/silver alloys⁴³. For the *monolayers* described in reference⁴³, this excess lateral density triggers defect formation in the substrate with loss of long-range order. Our results below however show that vertically-interdigitated bilayered films with this density on V_2O_5 favor the experimentally-observed interlayer space. The computed molecular dynamics structures (Figure 3) then provide the atom-scale features of the layered structure revealed by electron microscopy (Figure 2).

In contrast to alkanethiol self-assembly on metals, the metal oxide V_2O_5 (010) substrate features oxygen-bridged vanadium binding sites³⁰. This constraint gives the packing arrangements shown in Figure 3. The computed inter-sulphur distances given in Figure 4a show how, relative to a reference water-solvated dodecanethiol bilayer with S---S contacts of 0.41 nm³³, the substrate imposes alternately cramped (0.37 nm) and sparse (0.51-0.72 nm) arrangements on the thiol headgroups.

We tested the plausibility of the interdigitated assembly by considering also an alternative model (Figure 4b) in which the chains tilt rather than interdigitate. These alternative models (listed in Table 1) use the chain attachment schemes **A**, **B** and **C** (Figure 1a(ii)) with configuration **A*** also tested for the non-interdigitated model, an orientation whereby the monolayers are not aligned vertically but juxtaposed with opposing tilt angles. The computed preference for interdigitation is approximately $-5 \pm$

1
2 1 kcal/mol per chain (Table 1, Sum values). The tilted arrangement thus constitutes a very low
3
4 probability state for the system. The preference arises largely from relief of molecular strain in the
5
6 interdigitated film, by -7 kcal/mol per chain (Table 1, bonded terms), and is consistent with the upright
7
8 chains observed in tunnelling microscopy images²¹.
9

10
11 Interdigitation then relieves conformational strain in the organic bilayer. Packing effects are less
12
13 important, with the 6 ± 2 kcal/mol loss in horizontal ordering in the interdigitated geometry offset by the
14
15 -4 ± 2 kcal/mol *improvement* in vertical contacts (Table 1, non-bonded components). Furthermore, the
16
17 2.5 nm structure promotes the moderate interdigitation that, relative to shorter 2.0 and longer 3.0 nm
18
19 spacings, both minimises strain and also improves inter-chain packing to within 2 kcal/mol of the non-
20
21 interdigitated arrangement (Table 1, non-bonded terms). The 2.5 nm interdigitated film maximises film
22
23 contacts, both horizontally along each substrate face and vertically between opposing substrate faces; for
24
25 long range layered order in these directions, an alkanethiol density that equates to bulk, substrate-free 2-
26
27 D and 3-D chain assemblies (Figure 1c) in addition to interdigitation is important. This three-
28
29 dimensional packing under the constraint of the $V_2O_5(010)$ crystallography underlies the formation of
30
31 stable intercalated films with the observed ~ 2.5 nm interlayer distances (Figure 2c); the stability of the
32
33 intercalated organic bilayer is primarily dictated by optimized packing densities. This value is in
34
35 between once and twice the length of a free extended dodecanethiol molecule (1.5 nm), highlighting the
36
37 reduction in interlayer space due to interdigitation.
38
39
40
41
42
43
44

45 The film stabilisation energies in Table 1 indicate a strong preference for the observed 2.5 nm
46
47 interlayer spacing for both of the alternative chain attachment schemes **A** and **B**, in agreement with the
48
49 available microscopy and diffraction data (Figure 2 and reference ²¹). The intermediate interlayer space
50
51 of 2.5 nm gives a significantly more stable film, with chain energies improved by 2-6 kcal/mol,
52
53 stemming from 1-2 kcal/mol benefits in chain conformations and also 1-5 kcal/mol from chain packing.
54
55 The largest penalties are for widening rather than narrowing the interlayer space. Components show that
56
57
58
59
60

1
2 the strongest driver towards 2.5 nm is the ~7 kcal/mol improvement in vertical chain interdigitation
3
4 compared to the wider 3.0 nm structure. Smaller benefits of 2-3 kcal/mol are obtained in *horizontal*
5
6 chain packing along each substrate face for 2.5 nm rather than the narrower 2.0 nm spacing.
7
8 Consideration then of the full 3-D packing explains the origin of the observed 2.5 nm spacing with the
9
10 requirement of a minimal packing density of the thiols on $V_2O_5(010)$ and chain interdigitation to form
11
12 the energetically preferable layered structure. The small empty pockets in the computed film structure
13
14 (Figure 3c(ii)) are a consequence of the dry environment approximation used in the simulations with all
15
16 alkanethiols bound to the substrate. These spaces may be occupied by solvent molecules in the
17
18 experimental synthesised fibers; for further discussion of chain hydration and chain
19
20 physisorption/diffusion in alkanethiol monolayers see references ^{35,38-39}, while vanadate surface
21
22 hydration, including chemisorption, is addressed in electronic structure studies, see for example,
23
24 references ²³⁻²⁴.

25
26
27
28
29
30 Conformational and packing effects share the penalties for narrowing of the interlayer space to
31
32 2.0 nm, with chain conformation contributing 45% in **A** and 51% in **B** (Table 1). For widening the space
33
34 to 3.0 nm, the packing penalty predominates, at 84% in **A** and 82% in **B**. The balance of film
35
36 conformation and packing effects is thus almost independent of the chain attachment scheme.
37
38 Arrangement **C** serves as a first approximation to a surface model with a mixture of reduced V^{4+} and
39
40 stoichiometric V^{5+} sites^{21,44}, which may favour a situation whereby for example, 4 of the 5 chains per
41
42 $[V_2O_5]_4$ unit point in the same direction to accommodate the large V^{4+} ion. The observed <10% V^{4+}
43
44 (above), means such **C** arrangements will have a low population in the fiber. In terms of packing, **C** has
45
46 both the lowest horizontal penalty and lowest vertical benefit (Table 1, non-bonded components)
47
48 compared with **A** and **B**. This reflects the V^{4+} -directed alternately sparse/dense distribution of chains on
49
50 opposing faces as shown in the thiol S---S separations in Figure 4a. The computed film energies reflect
51
52 the delicate balance between horizontal and vertical packing.
53
54
55
56
57
58
59
60

Atom-scale origin of the 2.5 nm interlayer spacing

Overall, the data shows how the interlayer spacing of 2.5 nm arises from a combination of optimised (a) chain orientations and horizontal, substrate-constrained contacts along each substrate face and (b) vertical contacts between faces. The most important insight from the data is that surfactant packing is one of the primary directors and maintainer of interlayer spacing. For all binding schemes **A**, **B** and **C** the simultaneous optimisation of packing in three dimensions stabilises the interlayer film. The three alternative arrangements **A**, **B** and **C** are essentially iso-energetic; all three may contribute to the layered structure. The optimal packing arrangement of the dodecanethiol chains is thus not a single periodic arrangement on V_2O_5 (010) but rather a mixture of states, lowering the sensitivity of the intercalated organic bilayer to the fine details of the substrate crystallography; the nature of the interlayer film directs the order in the layered structure. Organic layer defects³⁹ and vanadate hydration state⁴⁵⁻⁴⁶ may also affect the ultimate arrangement. The findings will also motivate extensions to account for detailed thiol binding and unbinding, and also dynamic redistribution of alkanethiols between those that are chemically-bound, those physisorbed to substrate, and those in bulk-like states outside the fiber, towards a highly descriptive model for V_2O_5 -alkanethiol assembly, and ultimately organic-inorganic hybrid layered materials in general.

The V_2O_5 directed surfactant assembly results in unusual three-dimensional packing arrangements that differ significantly from self-assembled monolayers formed on layered silicate and metal surfaces^{27,40,47}. In some features, the alkanethiols intercalated in V_2O_5 more resemble the molecular coats on low-diameter, curved nanoparticle surfaces⁴⁸⁻⁵⁰. The molecular dynamics model thus confirms, and extends, the major features observed in the microscopy experiments; in vanadium oxide-alkanethiol structures synthesised from gels, the film assembly dictates a 2.5 nm interlayer spacing. The simulations confirm that the lowest energy film is neither a simple bilayer nor a juxtaposition of two monolayers. The film forms an interdigitated structure, in agreement with near-atom scale microscopy images²¹ that show the surfactant chains in upright orientations in the 2.5 nm space. This arrangement,

1
2 when stacked as a superlattice, forms the layered structure, with the vertical interdigitation of
3
4 alkanethiols offsetting the horizontal packing penalty induced by the oxygen-bridged vanadium binding
5
6 sites.
7
8
9

10 11 **Conclusions**

12
13
14 The application of nanostructures in devices depends on the ability to organize them in complex
15
16 architectures and so atomic-scale descriptions may speed up development⁵¹⁻⁵². In the present work, we
17
18 presented new information on film structure in layered vanadium oxide, specifically the interdigitation
19
20 between monolayers on each substrate face to give the observed short interlayer spacing. One further
21
22 experimental test of the proposed interdigitated model could involve STM characterisation of exfoliated
23
24 layers to show the organic monolayer on the vanadium oxide basal plane. Harnessing these subtle
25
26 nanoscale effects may aid the production of nanostructured hybrid materials with physicochemical and
27
28 mechanical properties tailored for specific device applications. For example, a layered oxide structure
29
30 could be engineered to have, in organic solvent, non-interacting layers that become tightly-coupled upon
31
32 drying, a possible new nanomaterial for adhesives. For energy conversion and storage materials,
33
34 disentanglement of interdigitated films could be exploited to give a transducer that converts heat to
35
36 mechanical energy. In the nearer term, hybrid materials that uptake nanoparticles or sieve/intercalate
37
38 ions (*e.g.*, lithium-ion battery materials and sensors), may benefit from controlled interlayer spacings for
39
40 better filtration or incorporation of other inorganic materials. We hope that the results presented will
41
42 motivate further studies of vanadate and other layered structures, towards rational design that uses atom-
43
44 scale properties to direct architecture and function.
45
46
47
48
49
50

51
52
53 *Acknowledgements.* We acknowledge support from Science Foundation Ireland (SFI) under the Tyndall
54
55 National Access Programme, the INSPIRE programme funded by the Irish National Development Plan
56
57 2007-2013 and the European Community's Seventh Framework Programme (FP7/2007-2013) under
58
59
60

grant agreement n° 213382 (FUNMOL). We acknowledge SFI for computing resources at Tyndall National Institute and SFI/ Higher Education Authority for computing time at the Irish Centre for High-End Computing.

Supporting Information Available: HRTEM of dodecylamine-templated V₂O₅ nanotube layers, further discussion of film density, XPS of deposited nanofibers and HRTEM of surface thiol layers around nanofibers. This material is available free of charge *via* the Internet at <http://pubs.acs.org>.

References

- (1) Sanchez, C.; Julian, B.; Belleville, P.; Popall, M. *J. Mater. Chem.* 2005, 15, 3559-3592.
- (2) Pileni, M. P. *Nat. Mater.* 2003, 2, 145-150.
- (3) Shi, S. F.; Cao, M. H.; Fle, X. Y.; Xie, H. M. *Cryst. Growth Des.* 2007, 7, 1893-1897.
- (4) O'Hare, D.; Khan, A. I.; Ragavan, A.; Fong, B.; Markland, C.; O'Brien, M.; Dunbar, T. G.; Williams, G. R. *Ind. Eng. Chem. Res.* 2009, 48, 10196-10205.
- (5) Alivisatos, A. P. *Science* 1996, 271, 933-937.
- (6) Lieber, C. M.; Lu, W. *Nat. Mater.* 2007, 6, 841-850.
- (7) Decher, G. *Science* 1997, 277, 1232-1237.
- (8) Tenne, R.; Margulis, L.; Genut, M.; Hodes, G. *Nature* 1992, 360, 444-446.
- (9) Sanchez, C.; Grosso, D.; Soler-Illia, G. J. D. A.; Crepaldi, E. L.; Cagnol, F.; Sinturel, C.; Bourgeois, A.; Brunet-Bruneau, A.; Amenitsch, H.; Albouy, P. A. *Chem. Mater.* 2003, 15, 4562-4570.
- (10) Vossmeier, T.; Raible, I.; Burghard, M.; Schlecht, U.; Yasuda, A. *Sensors and Actuators B-Chemical* 2005, 106, 730-735.
- (11) Li, G.; Chu, C. W.; Shrotriya, V.; Huang, J.; Yang, Y. *Appl. Phys. Lett.* 2006, 88.
- (12) O'Dwyer, C.; Diaz, C.; Lavayen, V. *J. Solid State Chem.* 2010, 183, 1595-1603.
- (13) O'Dwyer, C.; Lavayen, V.; Tanner, D. A.; Newcomb, S. B.; Benavente, E.; Gonzalez, G.; Torres, C. M. S. *Adv. Funct. Mater.* 2009, 19, 1736-1745.
- (14) Coleman, J. N.; Lotya, M.; O'Neill, A.; Bergin, S. D.; King, P. J.; Khan, U.; Young, K.; Gaucher, A.; De, S.; Smith, R. J.; Shvets, I. V.; Arora, S. K.; Stanton, G.; Kim, H. Y.; Lee, K.; Kim, G. T.; Duesberg, G. S.; Hallam, T.; Boland, J. J.; Wang, J. J.; Donegan, J. F.; Grunlan, J. C.; Moriarty, G.; Shmeliov, A.; Nicholls, R. J.; Perkins, J. M.; Grieveson, E. M.; Theuvsissen, K.; McComb, D. W.; Nellist, P. D.; Nicolosi, V. *Science* 2011, 331, 568-571.
- (15) Xia, Y. N.; Yang, P. D.; Sun, Y. G.; Wu, Y. Y.; Mayers, B.; Gates, B.; Yin, Y. D.; Kim, F.; Yan, Y. Q. *Adv. Mater. (Weinheim, Ger.)* 2003, 15, 353-389.
- (16) Park, J.; Lee, E.; Lee, K. W.; Lee, C. E. *Appl. Phys. Lett.* 2006, 89, -.
- (17) Baik, J. M.; Kim, M. H.; Larson, C.; Yavuz, C. T.; Stucky, G. D.; Wodtke, A. M.; Moskovits, M. *Nano Lett.* 2009, 9, 3980-3984.
- (18) Wu, C. Z.; Xie, Y. *Energy & Environmental Science* 2010, 3, 1191-1206.
- (19) Livage, J. *Chem. Mater.* 1991, 3, 578-593.
- (20) Selloni, A.; Sun, C. H.; Liu, L. M.; Lu, G. Q.; Smith, S. C. *J. Mater. Chem.* 2010, 20, 10319-10334.
- (21) O'Dwyer, C.; Lavayen, V.; Fuenzalida, D.; Lozano, H.; Santa Ana, M. A.; Benavente, E.; Gonzalez, G.; Torres, C. M. S. *Small* 2008, 4, 990-1000.
- (22) Chirayil, T.; Zavalij, P. Y.; Whittingham, M. S. *Chem. Mater.* 1998, 10, 2629-2640.
- (23) Yin, X. L.; Han, H. M.; Gunji, I.; Endou, A.; Ammal, S. S. C.; Kubo, M.; Miyamoto, A. *J. Phys. Chem. B* 1999, 103, 4701-4706.
- (24) Thompson, D.; Hodnett, B. K. *Top. Catal.* 2008, 50, 116-123.
- (25) Casal, B.; Ruizhitzky, E.; Crespin, M.; Tinetti, D.; Galvan, J. C. *Journal of the Chemical Society-Faraday Transactions I* 1989, 85, 4167-4177.
- (26) Lavayen, V.; O'Dwyer, C.; Santa Ana, M. A.; Newcomb, S. B.; Benavente, E.; Gonzalez, G.; Torres, C. M. S. *Physica Status Solidi B-Basic Solid State Physics* 2006, 243, 3285-3289.
- (27) Heinz, H.; Castelijns, H. J.; Suter, U. W. *J. Am. Chem. Soc.* 2003, 125, 9500-9510.
- (28) Parr, R. G.; Yang, W. T. *J. Am. Chem. Soc.* 1984, 106, 4049-4050.
- (29) Gronbeck, H.; Curioni, A.; Andreoni, W. *J. Am. Chem. Soc.* 2000, 122, 3839-3842.
- (30) Wyckoff, R. W. G. *Crystal structures*; R.E. Krieger Pub. Co.: Malabar, Fla., 1982.
- (31) CRC Handbook of Chemistry and Physics, 77th ed.; CRC Press: New York, 1996-1997.
- (32) Sigma-Aldrich online catalogue entry for 1-dodecanethiol at http://www.sigmaaldrich.com/catalog/ProductDetail.do?D7=0&N5=SEARCH_CONCAT_PNO|BRAND_KEY&N4=471364|ALDRICH&N25=0&Q_S=ON&F=SPEC. Accessed July 26 2011.
- (33) MacKerell, A. D.; Bashford, D.; Bellott, M.; Dunbrack, R. L.; Evanseck, J. D.; Field, M. J.; Fischer, S.; Gao, J.; Guo, H.; Ha, S.; Joseph-McCarthy, D.; Kuchnir, L.; Kuczera, K.; Lau, F. T. K.; Mattos, C.; Michnick, S.; Ngo, T.; Nguyen, D. T.; Prodhom, B.; Reiher, W. E.; Roux, B.; Schlenkrich, M.; Smith, J. C.; Stote, R.; Straub, J.; Watanabe, M.; Wiorkiewicz-Kuczera, J.; Yin, D.; Karplus, M. *J. Phys. Chem. B* 1998, 102, 3586-3616.

- 1
2
3
4
5
6
7
8
9
10
11
12
13
14
15
16
17
18
19
20
21
22
23
24
25
26
27
28
29
30
31
32
33
34
35
36
37
38
39
40
41
42
43
44
45
46
47
48
49
50
51
52
53
54
55
56
57
58
59
60
- (34) Petkov, V.; Trikalitis, P. N.; Bozin, E. S.; Billinge, S. J. L.; Vogt, T.; Kanatzidis, M. G. *J. Am. Chem. Soc.* 2002, *124*, 10157-10162.
- (35) Gannon, G.; Larsson, J. A.; Thompson, D. *J. Phys. Chem. C* 2009, *113*, 7298-7304.
- (36) Phillips, J. C.; Braun, R.; Wang, W.; Gumbart, J.; Tajkhorshid, E.; Villa, E.; Chipot, C.; Skeel, R. D.; Kale, L.; Schulten, K. *J. Comput. Chem.* 2005, *26*, 1781-1802.
- (37) Ryckaert, J. P.; Ciccotti, G.; Berendsen, H. J. C. *J. Comput. Phys.* 1977, *23*, 327-341.
- (38) Gannon, G.; Larsson, J. A.; Greer, J. C.; Thompson, D. *Langmuir* 2009, *25*, 242-247.
- (39) Gannon, G.; Greer, J. C.; Larsson, J. A.; Thompson, D. *ACS Nano* 2010, *4*, 921-932.
- (40) Love, J. C.; Estroff, L. A.; Kriebel, J. K.; Nuzzo, R. G.; Whitesides, G. M. *Chem. Rev. (Washington, DC, U. S.)* 2005, *105*, 1103-1169.
- (41) Humphrey, W.; Dalke, A.; Schulten, K. *Journal of Molecular Graphics* 1996, *14*, 33-&.
- (42) Giorgetti, M.; Passerini, S.; Smyrl, W. H.; Berrettoni, M. *Inorg. Chem.* 2000, *39*, 1514-1517.
- (43) Kawasaki, M.; Iino, M. *J. Phys. Chem. B* 2006, *110*, 21124-21130.
- (44) Avansi, W.; Ribeiro, C.; Leite, E. R.; Mastelaro, V. R. *Cryst. Growth Des.* 2009, *9*, 3626-3631.
- (45) O'Dwyer, C.; Lavayen, V.; Newcomb, S. B.; Ana, M. A. S.; Benavente, E.; Gonzalez, G.; Torres, C. M. S. *J. Electrochem. Soc.* 2007, *154*, K29-K35.
- (46) Livage, J. *Nat. Mater.* 2003, *2*, 297-299.
- (47) Heinz, H.; Vaia, R. A.; Farmer, B. L. *Langmuir* 2008, *24*, 3727-3733.
- (48) Badia, A.; Cuccia, L.; Demers, L.; Morin, F.; Lennox, R. B. *J. Am. Chem. Soc.* 1997, *119*, 2682-2692.
- (49) Wang, L. Y.; Shi, X. J.; Kariuki, N. N.; Schadt, M.; Wang, G. R.; Rendeng, Q.; Choi, J.; Luo, J.; Lu, S.; Zhong, C. J. *J. Am. Chem. Soc.* 2007, *129*, 2161-2170.
- (50) Wang, J. C.; Neogi, P.; Forciniti, D. *J. Chem. Phys.* 2006, *125*, -.
- (51) Perl, A.; Gomez-Casado, A.; Thompson, D.; Dam, H. H.; Jonkheijm, P.; Reinhoudt, D. N.; Huskens, J. *Nature Chem.* 2011, *3*, 317-322.
- (52) Noy, A. *Adv. Mater. (Weinheim, Ger.)* 2011, *23*, 807-820.

Table 1. Computed film stabilities (kcal/mol) in dodecanethiol-V₂O₅ nanostructures for two film geometries and a range of interlayer spacings and chain binding arrangements. Total film energies obtained at 2.5 nm layer spacing are given in bold.

Inter-layer space (nm)	Chain binding scheme	Film energies per dodecanethiol chain			Non-bonded components	
		bonded	non-bonded	Sum	horizontal	vertical
Interdigitated film geometry						
2.0	A	+26.6	-13.4	+13.2	-4.4	-9.0
2.5		+25.2	-15.2	+10.0	-7.8	-7.4
3.0		+26.2	-10.2	+15.9	-9.2	-1.0
2.0	B	+26.0	-14.5	+11.5	-5.2	-9.3
2.5		+25.2	-15.2	+10.0	-7.3	-7.9
3.0		+26.2	-10.6	+15.6	-9.5	-1.1
2.5	C	+25.4	-15.4	+9.9	-10.9	-4.5
Control simulations with non-interdigitated film geometry						
2.5	A	+32.3	-16.9	+15.4	-14.0	-2.9
2.5	A*	+32.1	-17.0	+15.1	-14.4	-2.6
2.5	B	+32.4	-17.4	+15.0	-14.5	-2.9
2.5	C	+31.9	-17.9	+13.9	-15.8	-2.1

Film energies computed from the final 2 ns (1000 structures) of 5 ns room temperature molecular dynamics; full computational details are in Supporting Information, section S1.5. A minus sign indicates film stabilisation. Time-averaged standard deviations are <0.2 kcal/mol. Chain attachment schemes are described in the text. Bonded and non-bonded energy terms quantify the conformational energy of the chains and the packing interactions between the chains. The large positive bonded terms reflect the inherent strain in alkanethiol assemblies, with similarly large bonded energy terms of 25.7±0.1 kcal/mol computed for bulk dodecanethiol chains³⁸. Non-bonded components are computed by averaging over chains along each substrate face (horizontal) and between chains on opposing faces (vertical).

Figure captions

Figure 1. Panel (a)(i) shows the V_2O_5 unit cell³⁰, composed of a V_4O_{10} repeat unit with lattice parameters $a = 11.51$, $b = 3.56$ and $c = 4.37$ Å (space group $Pmmn$), together with (ii) plan view schematics of V_2O_5 (010) functionalized with three alternative alkanethiol attachment schemes **A**, **B** and **C**. Black full circles represent alkane chains pointing up and black empty circles represent alkane chains pointing down. Panel (b) shows one representative computed nanofiber structure, for configuration **A** with interlamellar space of 2.0 nm. Chains on opposite substrate faces are coloured blue and yellow. Surrounding periodic images are coloured grey. Panel (c) shows how chain density changes with interlamellar spacing. The square and circular datapoints (lefthand and righthand axes) show the change in chain packing densities, expressed as chains/nm² and g/cm³; the grey and blue dashed lines mark the computed chain density in the reference water-solvated bilayer and bulk liquid.

Figure 2. (a) SEM image of as-synthesized V_2O_5 nanofibers (*inset*) plan view TEM image of several crystalline nanofibers. (b) Plan view TEM of several nanofibers overlapping (*inset*) HRTEM image showing the single crystal nature of the nanofiber. (c) HRTEM image of the cross section of a single nanofiber showing the ordered, layered structure. The interlayer spacing is 2.40–2.55 nm. (d) Low angle X-ray diffraction (XRD) spectra of both the V_2O_5 xerogel and the V_2O_5 -alkanethiol layered product acquired with grazing incidence geometry. (e) Schematic representation of the layered nanostructure. Regions 1 (plan view) and 2 (cross-section) correspond to the TEM images in (a) and (c) respectively.

Figure 3. Panels (a), (b) and (c)(i) show representative molecular dynamics snapshots. Only chains within ± 3 nm of the center are shown, with chains on opposite substrate faces colored blue and yellow. Chains are shown as bonds with a terminal sulphur sphere while V_2O_5 (010) is shown as green vanadium and red oxygen spheres. Panel (c)(ii) shows an alternative representation of one model with space-filling spheres.

Figure 4. (a) Radial distribution functions (RDF) for thiol S---S separations on each substrate face,

1
2 compared with the perfect packing obtained in water. **(b)** Reference non-interdigitated structures in
3
4 configurations *(i)* **A**, *(ii)* **A***, *(iii)* **B** and *(iv)* **C**.
5
6
7
8
9
10
11
12
13
14
15
16
17
18
19
20
21
22
23
24
25
26
27
28
29
30
31
32
33
34
35
36
37
38
39
40
41
42
43
44
45
46
47
48
49
50
51
52
53
54
55
56
57
58
59
60

Figure 1

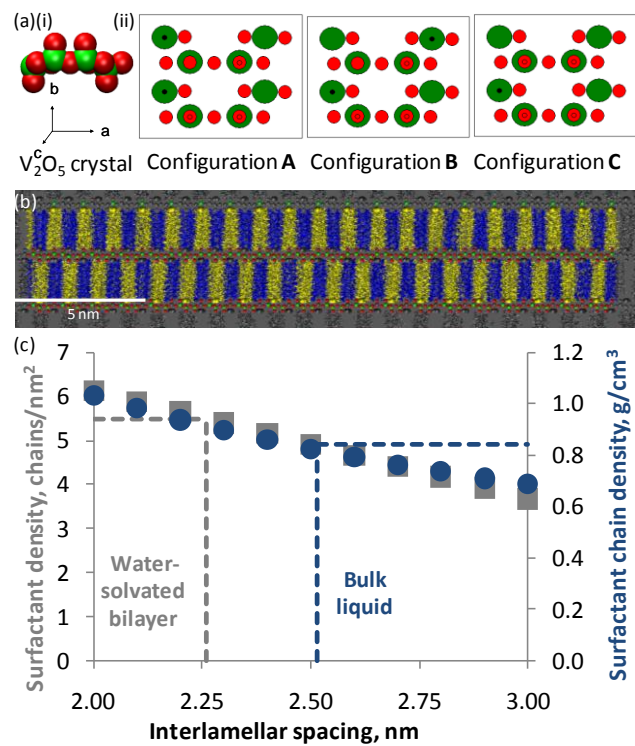


Figure 2

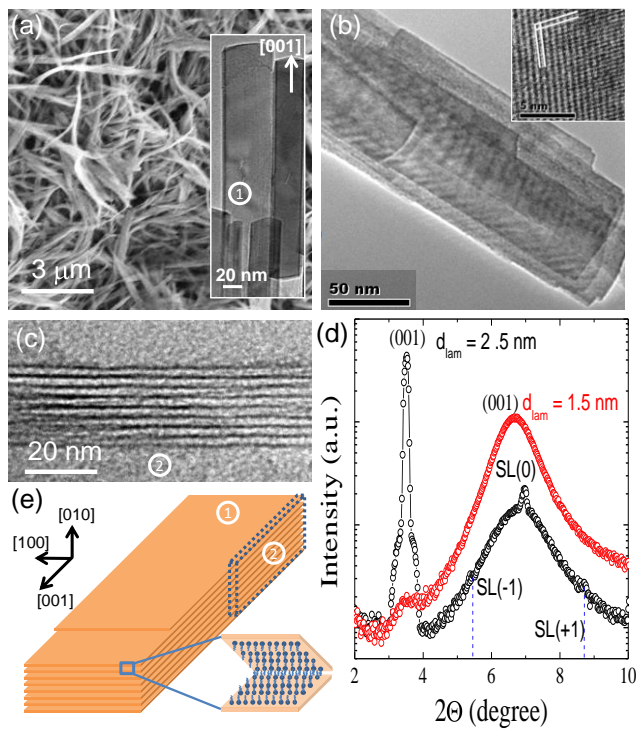


Figure 3

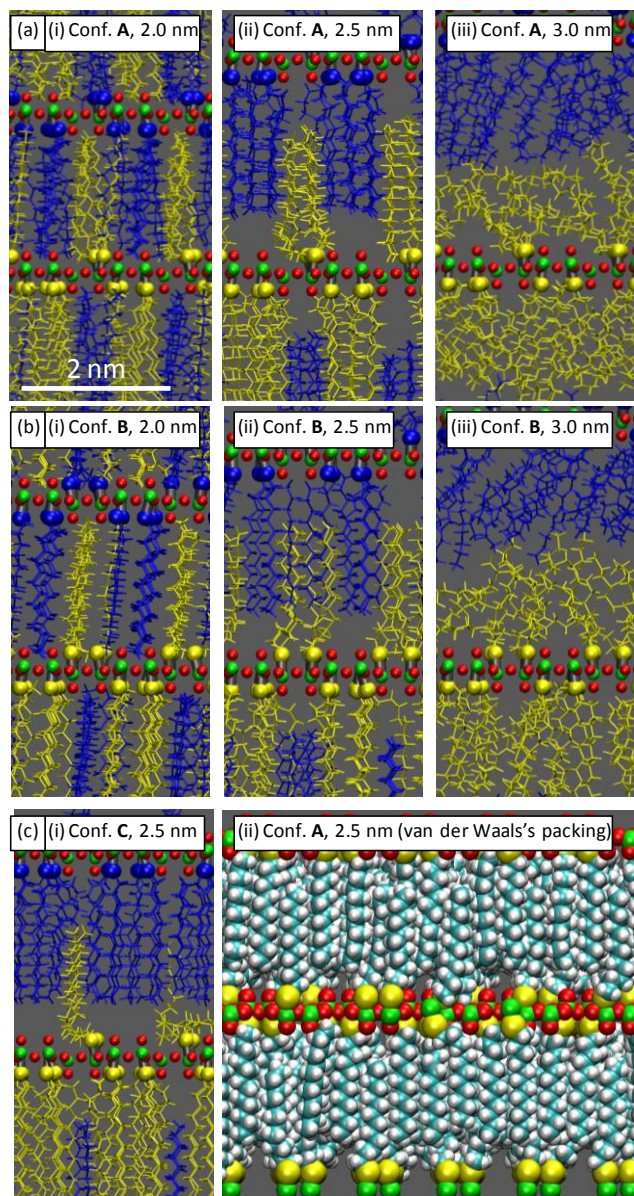


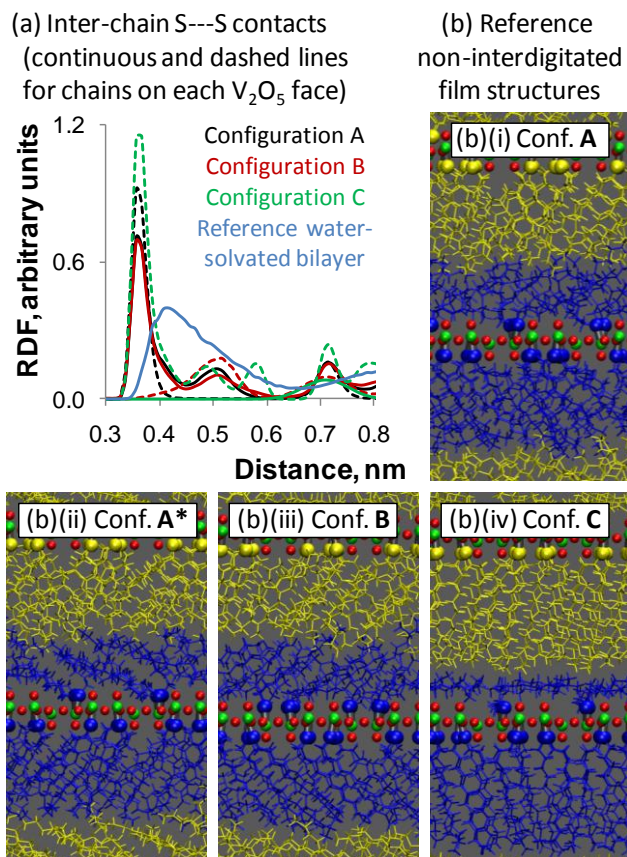
Figure 4

Table of Contents Image

